Yiwen Fang, Jonathan R. Dilworth, Michael Pepper and Peter P. Edwards*

Investigations of the optical and electronic effects of silicon and indium co-doping on ZnO thin films deposited by spray pyrolysis

https://doi.org/10.1515/znb-2019-0196
Received November 18, 2019; accepted November 28, 2019

Abstract: Silicon and indium co-doped ZnO thin films with both high optical and electrical performances have been successfully synthesised for the first time by the technique of spray pyrolysis. We find that this co-doping strategy can achieve comparable Figures-of-Merit performances to indium zinc oxide itself, but with, importantly, a significant saving in the indium content. The properties of the co-doped films are compared with those of either single indium or silicon doping.

Keywords: doping; Figures-of-Merit; indium; silicon; spray pyrolysis; thin film; transparent conducting oxide; zinc oxide.

Dedicated to: Professor Arndt Simon on the occasion of his 80th birthday. One of us (PPE) has had the honour – and the pleasure – of knowing and interacting with Arndt Simon for over four decades. His seminal studies have led to numerous unknown compounds and new compound classes. His elegant work has naturally, effortlessly and effectively combined solid state chemistry, physics and materials science in a way that has been, and continues to be, an inspiration to all of us who search for frontiers across the boundaries of those disciplines. A multitude of sincere and heartfelt thanks, Arndt!

1 Introduction

Indium-based transparent conducting oxides (TCOs) such as indium tin oxide (ITO) are widely used in optoelectronic devices and an important goal is to search for high-performance TCOs that have reduced or indeed zero indium contents. The inexpensive zinc-based TCOs have been shown to be good candidates to replace expensive indium-based films in a wide range of applications [1–4]. We have investigated if the indium content – and therefore cost of IZO films – could be reduced while maintaining the optoelectronic performance by the approach of co-doping with silicon. Here we have focussed on the vacuum-free, lower-cost spray pyrolysis technique for thin film fabrication.

Our group has previously [5, 6] successfully synthesised high-performance Si doped ZnO (SiZO) thin films by spray pyrolysis and also [7–9] analysed the performance and limitations of Si doped zinc-based TCOs, as have others, using a variety of deposition techniques [10–14]. Calculations on the electronic band structure of SiZO have also been reported [15, 16]. However, the best SiZO films deposited by spray pyrolysis only have conductivities of ca 200 Ω^{-1} cm^{-1} and carrier concentrations of ca. 1.2×10^{20} cm^{-3} although those films prepared from sputtering have somewhat higher values of these transport properties. In-doped ZnO (IZO) films deposited either by sputtering or spray pyrolysis have been investigated extensively [17–26] and the films produced by spray pyrolysis show conductivities of the order of 700 Ω^{-1} cm^{-1} and carrier concentrations around 3.2×10^{20} cm^{-3}. We have investigated whether co-doping with both Si and In together can enable the spray deposition of films which reduce the In content whilst also maintaining the overall electrical and optical performance. Si and In co-doped films have previously been deposited as amorphous films by magnetron sputtering [27, 28] but not by spray pyrolysis. In this work two series of doped ZnO films were deposited: The first with Si and In had concentrations of 0.6% and 0–7%, respectively, and the second series had In and Si concentrations of 2% and 0–7%, respectively. We note that the concentrations reported throughout are those present in the films as determined by ICP-MS. The concentrations of dopant in the films was also measured by EDX using a cross section of the film and these values are broadly comparable to those obtained by ICP-MS, although they did show some variation from the top to the bottom of the film.

***Corresponding author: Peter P. Edwards,** Inorganic Chemistry Laboratory, Department of Chemistry, University of Oxford, South Parks Road, Oxford OX1 3QR, UK,
e-mail: peter.edwards@chem.ox.ac.uk
Yiwen Fang and Jonathan R. Dilworth: Inorganic Chemistry Laboratory, Department of Chemistry, University of Oxford, South Parks Road, Oxford OX1 3QR, UK
Michael Pepper: London Centre for Nanotechnology and Department of Electronic and Electrical Engineering, University College London, Torrington Place, London, WC1E 7JE, UK

Brought to you by | UCL - University College London
Authenticated
Download Date | 2/18/20 6:41 PM

2 Results and discussion

2.1 Electrical properties

The precursor solutions used for the spray pyrolysis are as follows: zinc acetylacetonate was dissolved in 2:1 isopropanol/water and acidified with glacial acetic acid at the rate of one drop per 10 mL of solution. The appropriate amounts of silicon tetraacetate or indium trichoride were added to the zinc precursor solution and stirred for 24 h followed by filtration. A cleaned glass slide was placed on the heater bed and the whole apparatus purged with nitrogen. The slide was then heated to the deposition temperature and the precursor solutions sprayed at 0.55 mL per minute and when the required volume of precursor solution had been added allowed to cool to room temperature. The films were not annealed prior to the measurements.

The deposition temperature was optimised since electrical properties, especially mobilities and conductivites, of ZnO-based thin films are higly sensitive to film deposition temperature as discussed by Vai et al. [9]. Fixed temperature is neccessary to obtain films of stable and consistent quality. Films deposited at $T = 310°C$ have excelent and stable electrical properties; therefore it is chosen in this research. The thermal decomposition of zinc precursor is a complex process and a wide range of hydrocarbon and oxygenated hydrocarbon species can be observed by TOF-SIMS [29] but the final product is crystalline ZnO. The acetylacetonate ligand of zinc acetylacetonate is protonated and lost as acetylacetone which undergoes an alcoholysis reaction in an acidic solution and then produces acetone, isopropyl acetate, and Zn–OH species. Zn–OH species finally experience a condensation reaction and are converted into ZnO thin films [30].

The electrical properties of some 25 films are summarised in Figs. 1 and 2 and the data for each sample composition is averaged over at least three films. The carrier concentrations, mobilities and conductivities all show similar trends, rising to a maximum with increasing dopant concentration and decreasing thereafter. It has been shown [31, 33] that there is a thickness dependence of these parameters in doped ZnO films. However, all the doped films studied here have measured thicknesses between 620 and 680 nm, and the variation in the parameters over this range is small enough to be neglected. The maximum in both the carrier concentrations and mobilities represent a substitutional limit for effective doping, and beyond this point the dopant may occupy either interstitial or surface sites which are obviously unproductive in terms of increasing carrier concentration and hence conductivity.

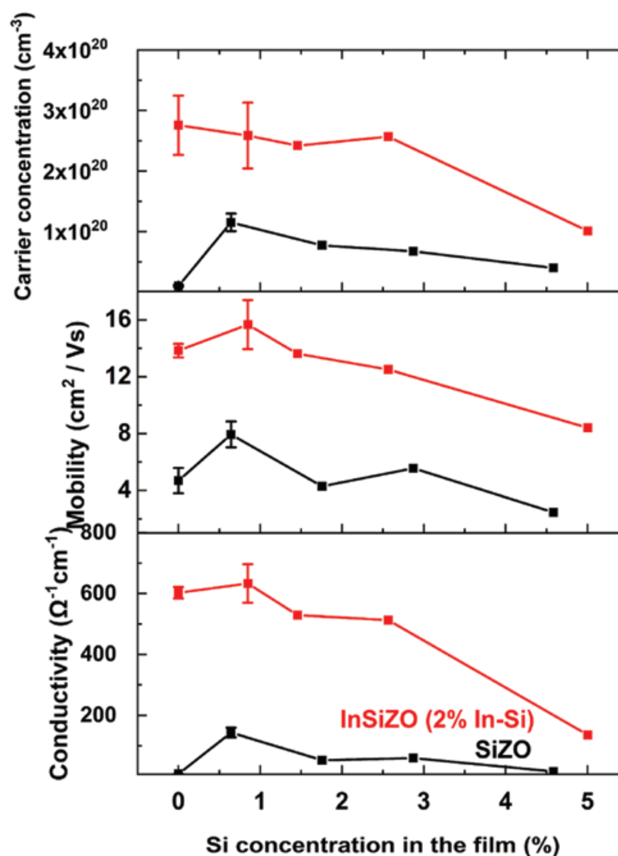

Fig. 1: Plots of measured carrier concentrations, mobilities and conductivities for films with a fixed In and various Si concentrations. Plots for SiZO are included for comparison.

The decrease in carrier mobility with increasing dopant level is attributable to the inevitable intervention of grain boundary scattering, ionic impurity scattering (including O defects) or the impact of an increasing electron-phonon interaction. The last are only significant in the far IR and can be neglected here [31, 34]. The inter-grain scattering may be reduced at high carrier concentrations due to quantum-mechanical tunnelling of the carriers through the potential energy barriers at the boundaries of crystallites, but this is offset by increased scattering from the increasing number of dopant cations and defects. The eventual drop in carrier concentration has been ascribed to the trapping of electrons at grain boundaries [9, 34] or possibly at positively charged but non-substitutional doping sites. The precise overall mechanism by which doping increases with carrier concentrations is still a matter for discussion. There are suggestions in the literature that the additional electrons originate from silicon itself, but the 2*s* and 2*p* orbitals of the Si^{4+} ion are energetically inaccessible. A more plausible explanation is that the increase in positive charge by replacing Zn^{2+} with an ion with a higher charge requires the

Brought to you by | UCL - University College London
Authenticated
Download Date | 2/18/20 6:41 PM

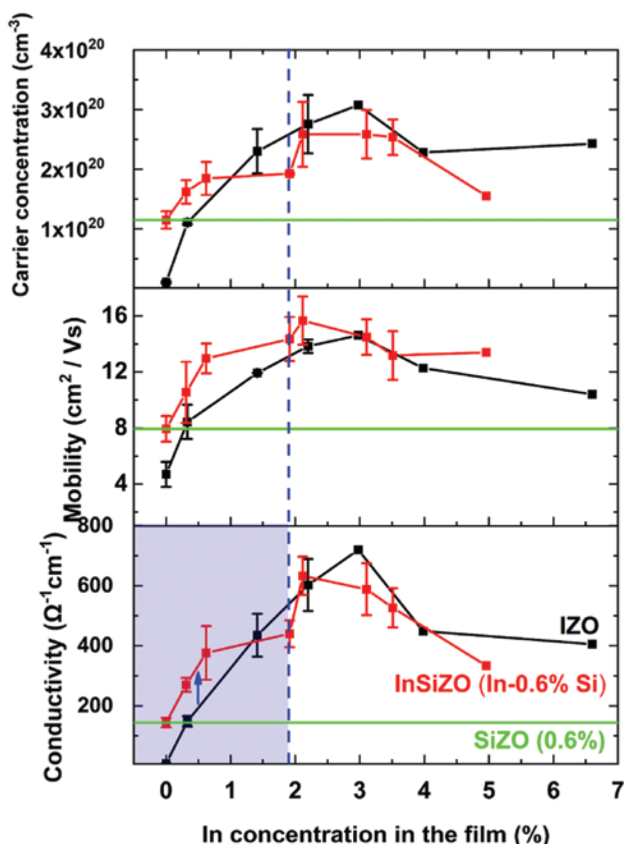

Fig. 2: Plots of measured carrier concentrations, mobilities and conductivities for films with fixed Si and various indium film concentrations. Plots for IZO are included for comparison.

natural acquisition of additional oxide anions to maintain charge neutrality. Subsequent loss of these oxide anions as gaseous oxygen under slightly reducing conditions generates oxygen defects and two electrons and these additional electrons can be located in an impurity band or the host (ZnO) conduction band. High resolution XPS spectroscopy [35] has shown that the number of O defects increases at higher dopant concentrations in accord with the above model. Although the formation of O vacancies or defects undoubtedly contributes to the improvements in the electrical properties on doping, other factors such as changes in both physical and band structures can also play a role.

For the singly doped IZO and SiZO films, Figs. 1 and 2 show that In is generally a much more effective dopant than Si. Thus, the film with 0.6% In has a conductivity of 230 Ω^{-1} cm^{-1} compared to 140 Ω^{-1} cm^{-1} for the film with the same amount of Si. Since the charge on In^{3+} is less than Si^{4+} this confirms that the beneficial effects of In doping are not solely due to the formation of O defects via charge neutralisation. This divergence increases with dopant concentration; at 3% the conductivities for the Si and In doped films are 80 and 700 Ω^{-1} cm^{-1}, respectively. The effects may have their origin in the better size match of In^{3+} (0.62 Å) with Zn^{2+} (0.6 Å) than Si^{4+} (0.26 Å) and the energy and larger spatial size of the In 5*s* orbital compared to the Si 3*s* and 3*p* orbitals [36].

For the InSiZO films (Fig. 2) the conductivities are highest for around 2% In with 0.6% Si (the value for SiZO which gives the maximum carrier concentrations and conductivities) and lie close to the values for IZO. At 3% In in IZO the conductivity rises to a maximum as do the carrier mobilities and concentrations. In the range of 2–3% In, the carrier concentrations and conductivities for InSiZO are lower than for IZO suggesting an inhibitory effect for the 0.6% Si present. However, the error bars for the InSiZO are quite large here. At In concentrations in the 0–2% region (shaded blue in the figure) InSiZO has, as expected, significantly better electrical performance than IZO. Interestingly there does not appear to be a competition between Si and In for substitutional sites, for when the precursor Si concentration is held steady the film concentration of Si does not decrease as the In concentration is ramped up.

Thus, if one was just seeking the optimal electrical performance regardless of factors such as cost and transparency, IZO with ca. 3% In content would be selected. However, as discussed below if the additional factors such as transparency and costs are considered then the choice would naturally switch to InSiZO.

2.2 Optical properties

UV transmission spectra for ZnO, IZO and InSiZO films are shown in Fig. 3a and c over the wavelength range 500–2500 nm. Importantly, the data in the Table S1 (Supporting information available online) show that the presence of silicon as a dopant improves the transmittance (determined by the Swanepoel technique) which shows a dramatic decrease above 1000 cm^{-1} as the dopant concentrations in the films increase due to the higher carrier concentrations which leads to reflectance in the NIR region and a shift of the plasma frequency to shorter wavelengths. The inset plots of band gap (derived from Tauc plots) show that the band gap increases fairly uniformly with increasing In dopant concentrations as found by others for IZO films [37]. The incorporation of Si (Fig. 3b and d) appears to have little impact on the final magnitude of the band gap [38] (in the range of 2% In and higher) in the visible region. The SiZO film with 0.6% Si has the highest transmittance and the incorporation of In in the InSiZO films causes a drop in the average transmittance, which is is still higher than for IZO in the 0–3% In concentration range.

Brought to you by | UCL - University College London
Authenticated
Download Date | 2/18/20 6:41 PM

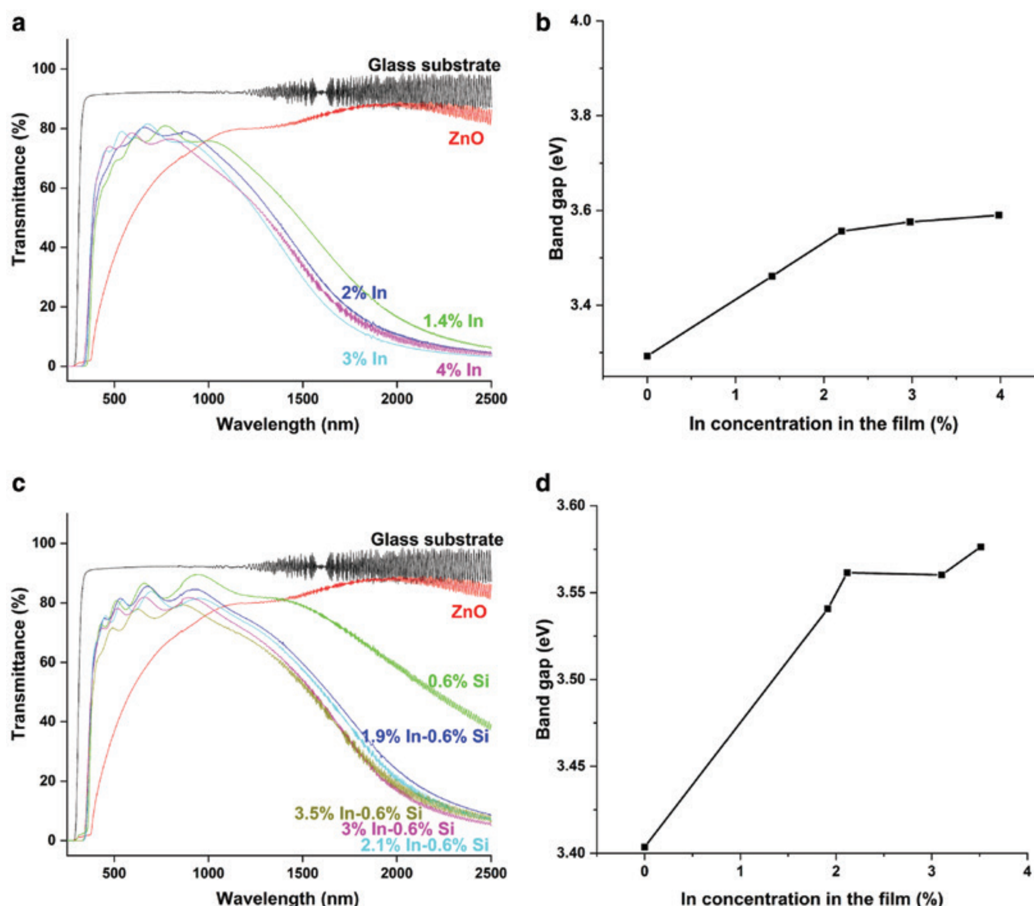

Fig. 3: Transmission UV/visible spectra for IZO films with various In concentrations (a) and InSiZO films with fixed Si and various In contents (c). Corresponding band gaps for (a) and (c) are shown as (b) and (d), respectively.

The Lorenz oscillator model and the modified Drude equation [31] were used to calculate key parameters for reflection spectra and the WVASE programme (J. A. Woollam Co.) [32] was employed to simulate the observed reflectance spectra. A typical reflectance spectrum for SiZO with 0.6% Si is shown in Fig. 4 in black with the simulated spectrum as a dashed red line. The data from the WVASE programme was then used to calculate optical carrier concentrations, mobilities and conductivities, and this data for all of the films is plotted together with the data derived from the Hall effect measurements displayed in Fig. 5.

The measured dc Hall mobility is the sum of both the inter- and intra-grain mobilities whereas the optical mobility relates solely to the mobility of carriers within the interiors of the grains. The difference between the two mobilities therefore reflects the impact of the grain boundaries on electron transport. Generally, the data contained in the figures suggest that the inter-grain boundary effects are less pronounced for In than for Si and tend to increase with the amount of dopant(s) added. The plots for InSiZO are similar to those for IZO again confirming that the presence of In dominates the electrical properties.

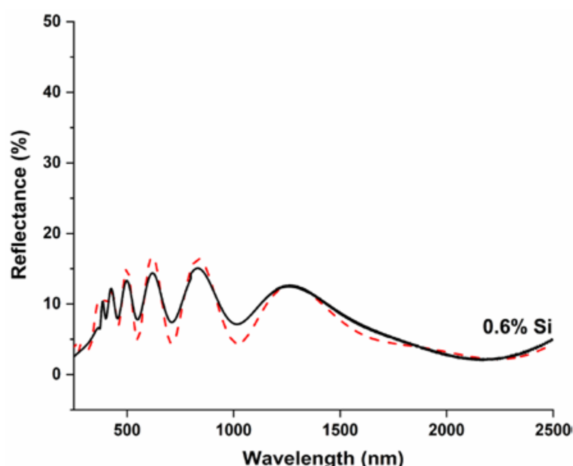

Fig. 4: A typical UV-Vis-NIR optical reflectance spectrum of SiZO (0.6%) thin films, together with the computed reflectance spectrum (red dotted line).

For all three plots the optical carrier concentrations do not fall as rapidly with increasing dopant as those measured by the dc Hall effect as there is no trapping of electrons at the grain boundaries.

Brought to you by | UCL - University College London
Authenticated
Download Date | 2/18/20 6:41 PM

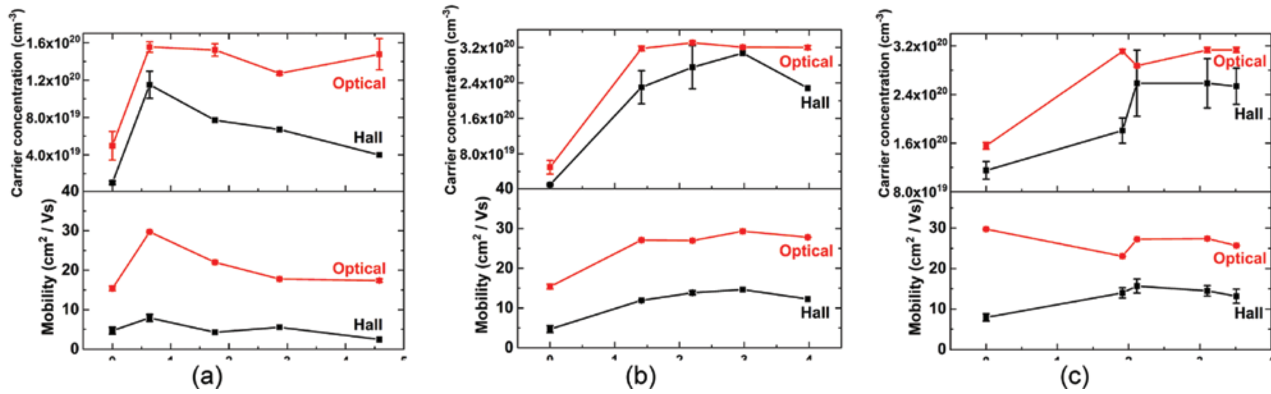

Fig. 5: Optical (red) and Hall (black) electrical properties of SiZO (a), IZO (b), and InSiZO (In-0.6% Si) (c) thin films.

2.3 Structural studies

2.3.1 XRD

The XRD patterns for SiZO (a), IZO (b) and InSiZO (c) are shown in Fig. 6. For the SiZO films the XRD shows that the growth orientation is along the 002 plane as in ZnO although there is some of the 101 plane orientation at lower concentrations. By contrast the addition of In the 002 plane of ZnO is visible up to 3% In but is replaced by 101 and 100 planes at higher In concentrations. InSiZO is similar to IZO again showing that In substitution dominates over Si in determining the crystal growth orientations.

The lattice parameters and unit cell volumes for the various samples are shown in Fig. 7. The data for SiZO shows that the unit cell volume and lattice parameter for the $a=b$ axis both decrease up to ca. 0.6% Si as expected if the much smaller Si^{4+} substitutes for Zn^{2+}. Importantly, this Si concentration coincides with the maxima seen in the carrier concentrations. Thereafter there is an increase in both unit cell volume and lattice parameter $a=b$ consistent with the Si now being non-substitutional and located in interstitial sites. The situation for both IZO is that both the unit cell volume and lattice parameter increase steadily with increased In dopant. This fits with the picture that the better size match of In enables it to substitute for Zn^{2+} right up to a 4% concentration. For InSiZO the increase in unit cell volume is larger than for IZO and SiZO but also more irregular, but the reasons for this are not clear at this stage.

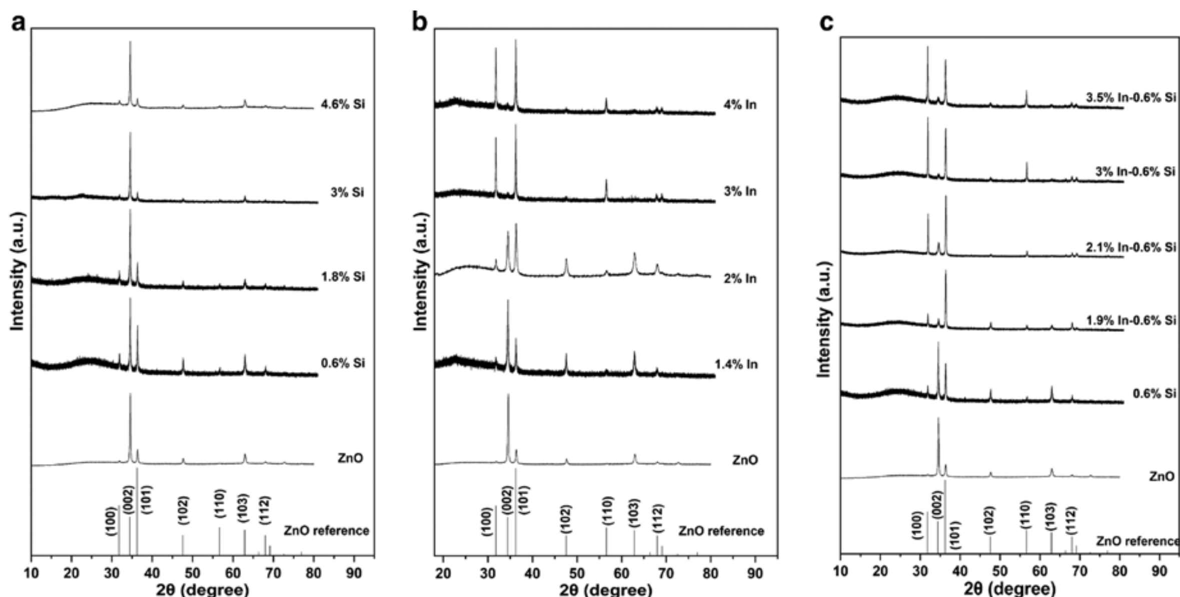

Fig. 6: XRD patterns of ZnO (a), IZO (b), and InSiZO (c) thin films.

Brought to you by | UCL - University College London
Authenticated
Download Date | 2/18/20 6:41 PM

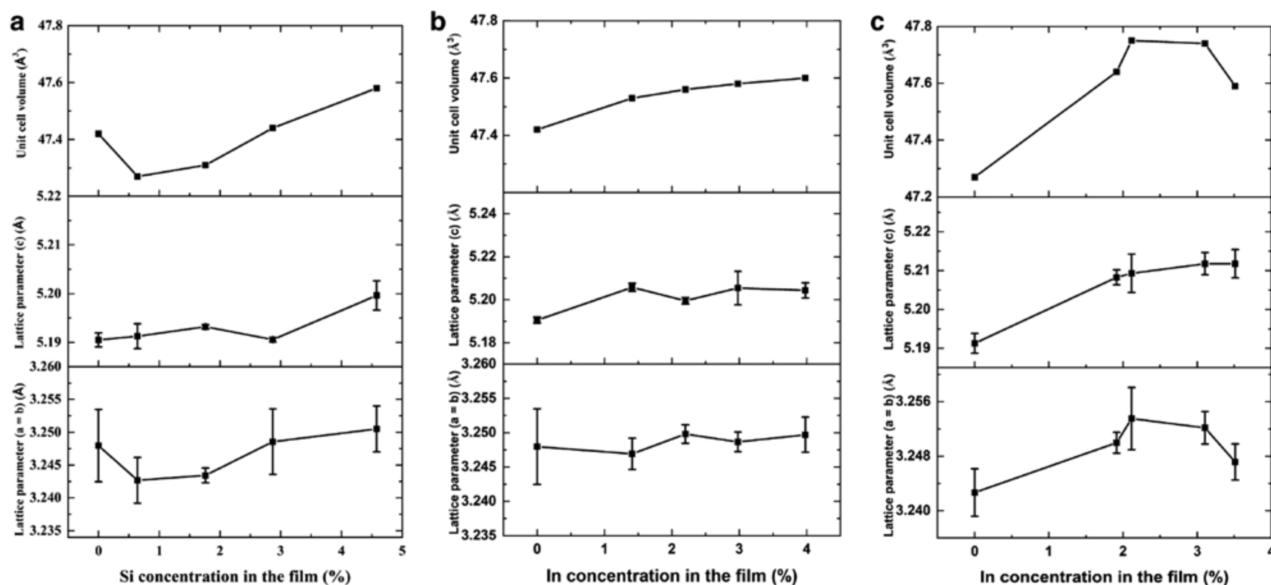

Fig. 7: Lattice parameters and unit cell volumes for SiZO (a), IZO (b) and InSiZO (c).

2.3.2 SEM

The SEM images of six films show significant changes in morphology when dopants are added and a tendency for the grain size to decrease as the dopant concentration rises. This trend is fairly linear for SiZO and InSiZO (Fig. 8 and Fig. S1; Supporting information) but more complex for InSiZO. The smaller grain size will lead to more grain boundaries which is consistent with the fall in carrier electron concentrations and mobilities observed at high dopant levels as shown in Figs. 1 and 2. However, the details of exactly how the introduction of dopant changes

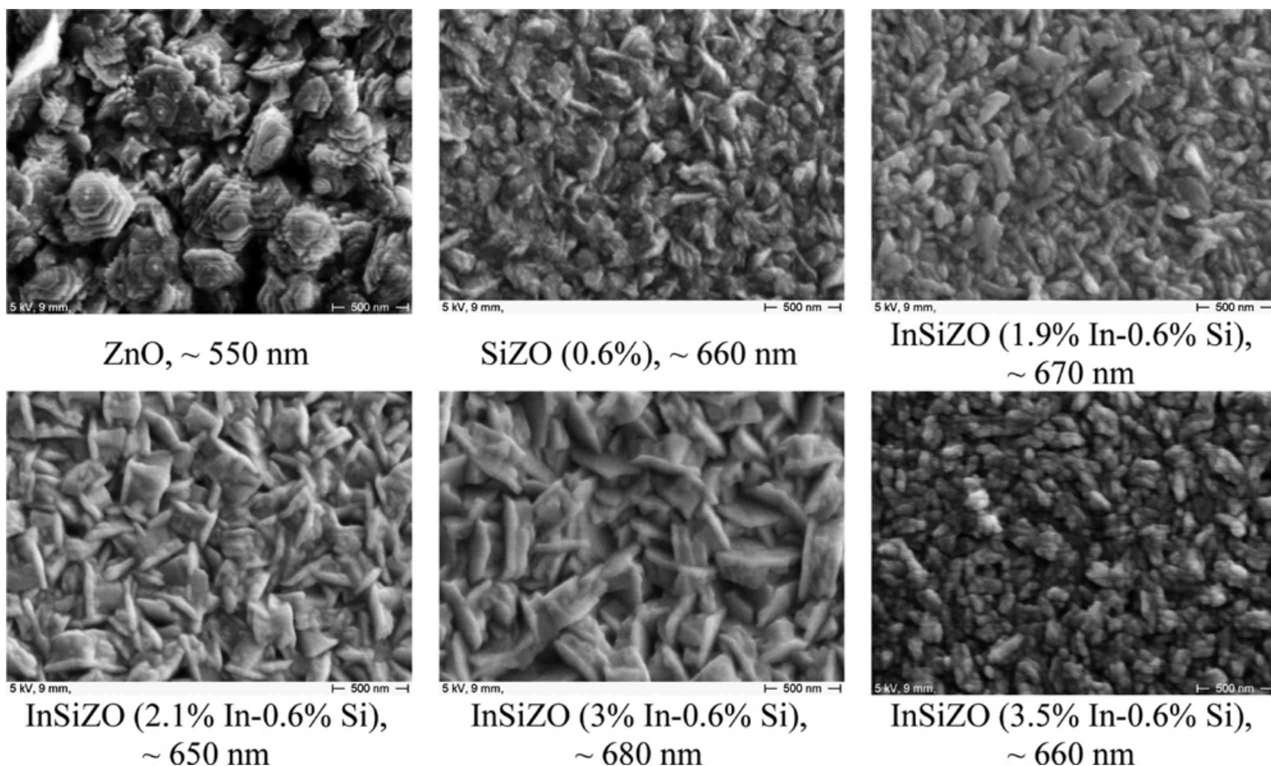

Fig. 8: SEM images of ZnO, SiZO and InSiZO films, the last with 0.6% Si and various In concentrations.

Brought to you by | UCL - University College London
Authenticated
Download Date | 2/18/20 6:41 PM

the morphology and grain size are not presently known. Similar trends have been observed for films deposited by sputtering techniques so the effect does not originate in using a solution-based deposition route.

3 Conclusions

Spray pyrolysis is shown to be an inexpensive and effective way to deposit singly (Si or In) and co-doped (Si and In) ZnO crystalline films on a glass substrate. The electrical properties for SiZO and IZO reported here compare well with literature values for solution-based deposition methods. All of the films show a similar trend in electrical properties with fall in values of both the carrier concentrations and mobilities beyond an optimal doping level. This is ascribed to the effects of grain boundaries and scattering due to doping ions and defects in the ZnO structure. The UV/visible spectra show good transparencies and a blue shift of the near IR absorbance which correlates with increasing carrier concentration. The observed separation between the calculated optical electrical properties and those determined by the Hall method is attributable at least in part to grain boundary effects. The XRD data shows that the crystal growth direction is dependent on the dopant. Si does not change the orientation from that of ZnO whereas In causes a shift of direction but only at higher In concentrations beyond the optimal value. These variations may well have an impact on the morphology changes observed by SEM. The cell volumes increase uniformly with higher In levels but for Si there is an initial decrease in cell volume up to a value of ca 0.6% Si which provides the optimum doping for the best electrical properties. Thereafter the cell volume increases consistent with the additional Si occupying other sites in the lattice. The SEM images in Fig. 8 and Figs. S1 and S3 (Supporting information) show that for IZO and SiZO there is a uniform reduction in grain size at higher concentrations of In or Si. However, for reasons not understood at present IZO shows a complex trend in grain size (see Figs. S2, S4 and S5; Supporting information).

Based purely on the electrical properties of singly doped ZnO, one would select IZO with 3% In as the highest performance film. In addition, 3% IZO also has the highest visible transmittance of 82% among IZO thin films. Therefore, 3% IZO is the best choice for both electrical and optical properties. However, for practical applications the important transparency in the visible region (400–700 nm) can be assessed by calculating the Figure-of-Merit (FOM) for the films using the formula proposed by Haacke [39]. If these FOM values are plotted for InSiZO films with a fixed Si concentration of 0.6% and variable levels of In, then the data presented in

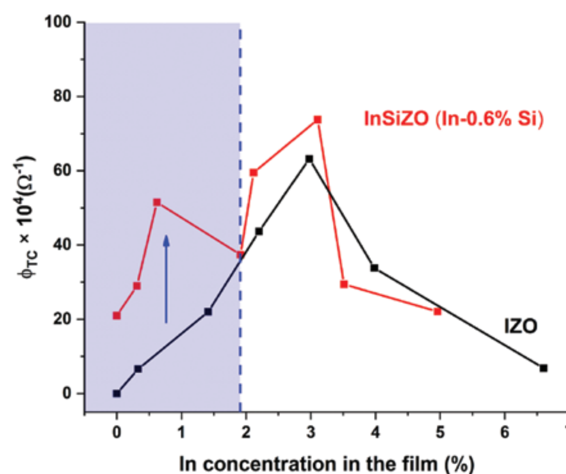

Fig. 9: Derived values of the Haacke Figure-of-Merit as a function of In concentration for the comparison of IZO and InSiZO thin films. The blue area highlights the superior optoelectronic performance of the investigated co-doped InSiZO thin films.

Fig. 9 is obtained. At In levels below 3% InSiZO is noticeably superior (higher FOM) due to the higher transparencies of the films containing Si. It is also possible to have a film with 80% of the FOM of the best IZO film with 0.6% Si and 0.6% In. These findings are consistent with those of Lim et al. [27] who reported that amorphous InSiZO films deposited by magnetron sputtering had a high enough transmittance for use in future transparent displays.

We note that this could obviously mean a large reduction in the amount of In used (ca. 2.5%) – and therefore with cost also – and with only a relatively modest drop in electrical properties but superior optical characteristics. This illustrates that InSiZO films would represent an acceptable, cost effective alternative to IZO itself in many applications, with even great potential in next-generation displays.

4 Experimental section

4.1 Materials and methods

Undoped and doped ZnO thin films were deposited by the spray pyrolysis technique at a specific substrate temperature. Undoped ZnO precursor solutions were prepared by dissolving zinc acetylacetonate hydrate ($Zn(C_5H_7O_2)_2 \, x \, H_2O$, 99.995% trace metals basis, Sigma-Aldrich) in a 2:1 volume ratio solvent of isopropanol ($(CH_3)_2CHOH$, ≥99.7%, Sigma-Aldrich) and distilled water (Ondeo Purite Select Analyst). The concentration of zinc acetylacetonate in the precursor solution was 0.15 mol L^{-1}. Ten droplets of glacial acetic acid (CH_3CO_2H, ≥99.7%, Alfa Aesar) were added to a 10 mL

Brought to you by | UCL - University College London
Authenticated
Download Date | 2/18/20 6:41 PM

precursor solution by using a 1 mL plastic Pasteur pipette to prevent any hydrolysis of zinc acetylacetonate. The precursor solution was stirred for 30 min to yield a clear solution before filtering through a qualitative filter paper (Whatman). The precursor solution should finally be clear and homogeneous. Ten millilitre of filtered precursor solution was used for each film deposition unless stated otherwise. To make films of different thicknesses, various volumes (0–10 mL) of precursor solutions were used for each film deposition.

To make SiZO precursor solutions, silicon tetraacetate ($Si(OCOCH_3)_4$, 98%, Sigma-Aldrich) was added to undoped ZnO precursor solutions prepared as above. The quantity of silicon tetraacetate added depended on molar ratios of Si and Zn (Si concentration = [Si]/[Zn] × 100%). The Si containing precursor solution was stirred for 24 h to yield a clear solution or a homogeneous mixture before filtering through a qualitative filter paper (Whatman). The precursor solution should finally be clear and homogeneous. IZO precursor solutions were made by adding indium chloride hydrate ($InCl_3$ x H_2O, 99.99% metals basis, Alfa Aesar) into undoped ZnO precursor solutions. Similarly, InSiZO precursor solutions were made by adding indium chloride hydrate ($InCl_3$ x H_2O, 99.99% metals basis, Alfa Aesar) and silicon tetraacetate ($Si(OCOCH_3)_4$, 98%, Sigma-Aldrich) into undoped ZnO precursor solutions. The quantities of starting materials added and the other procedures were the same as stated above.

Figure 10 shows the spray pyrolysis apparatus. The substrate was a 32 mm × 24 mm borosilicate glass rectangular coverslip (0.13–0.17 mm thick, Fisherbrand), which was cleaned in a mixture of distilled water and acetone by using an ultrasonic cleaner. The substrate was then dried at room temperature and further cleaned with a jet of pure dry nitrogen. The temperature of the heating platform as controlled by a Eurotherm PID temperature controller, and a thermocouple stainless steel probe was inserted into a small hole of the heating block. The heater surface temperature was kept at ~310°C during the spray pyrolysis. The precursor solution was pumped into an atomiser nozzle (BETE XA PR-050) by a syringe infusion pump (KDS 200 Legacy Dual Syringe Infusion Pump, KD Scientific) with a flow rate of 0.55 mL min^{-1}. 'House' dry nitrogen was used as the carrier gas to blow the precursor solution onto the glass substrate with a flow rate of 14.5 L min^{-1}. The distance between the nozzle and the glass substrate was 30 cm. The chamber was flushed with dry nitrogen to eliminate any air, and the heating platform was heated at a rate of 30 K min^{-1} and held at a specific deposition temperature for 20 min before pumping the precursor solution. The temperature was held for 5 min after finishing pumping the precursor solution. The heating platform was then cooled down to the room temperature at a rate of 25 K min^{-1} before the product was taken out of the chamber.

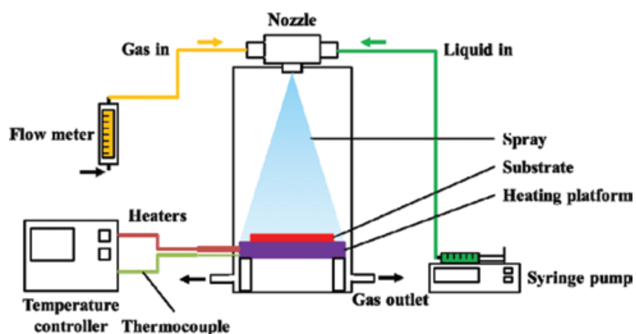

Fig. 10: Schematic of the spray pyrolysis process used in this investigation.

4.2 Characterisation techniques

TEM was carried out on a JEOL JEM-2010 Transmission Electron Microscope. It used a LaB_6 cathode at a beam energy of 200 keV. All images were taken on a Gatan 794 MultiScan camera. EDX spectra were taken on a Si(Li) Thermo Fisher EDX system. EDX spectra were acquired with an electron probe with a diameter of between 50 and 100 nm. The sample was tilted 15° towards the EDX detector to reduce X-ray shadowing. Three points were measured for each film, with collection times varying between 300 and 600 s per spectrum. UV-Vis-NIR spectroscopy was carried out on a PerkinElmer Lambda 19 UV/Vis/NIR spectrophotometer. It is a dual-beam spectrometer which can measure from about 175 to 3300 nm encompassing 95% of the solar spectrum. Its optical setup is double-beam, all-reflecting and double monochromator. The light source is a deuterium lamp for UV and halogen lamp for Vis/NIR, and the detector is PMT for UV/Vis and PbS for NIR. The spectra were collected at room temperature from 250 to 2500 nm with a data collection interval of 3 nm. UV-Vis-NIR reflectance spectroscopy was carried out on an Agilent Cary 5000 UV-Vis-NIR spectrometer. This is a dual-beam spectrometer which can measure from about 175 to 3300 nm. It uses a PbSmart NIR detector for an extended photometric range. It uses a floating Al casting and double Littrow monochromator to get minimal noise and stray light. It uses Schwarzschild coupling optics for higher accuracy at low transmission levels to get maximum light throughput. The dielectric function was carried out, calculated and modelled with the software WVASE (J. A. Woollam Co.) [32]. It is designed to fit optical spectra, such as reflectance, transmittance, ellipsometry, Drude-Lorentz, and many other dielectric-function models. Electrical properties (resistivity, carrier concentration and

Brought to you by | UCL - University College London
Authenticated
Download Date | 2/18/20 6:41 PM

mobility) were carried out by using van der Pauw and Hall Bar measurements on an Ecopia HMS-3000 Hall measurement system. The HMS-3000 includes software with I-V curve capability for checking the Ohmic integrity of the user made sample contacts. The systems can be used to characterise various materials from $T=300$ to 77 K (room temperature to liquid nitrogen temperature). The magnetic flux density is 0.55 T provided by permanent magnets. Thin film samples were mounted onto a PCB Sample Holder by annealing with a conductive material indium to ensure good probe contact to make four Ohmic contacts on the four corners of the thin films (5 mm × 5 mm). The input current is 1 nA–20 mA and 0.5 mA is normally used. The parameters are input (usually thin film thickness) and the output results can be carrier concentration, mobility, resistivity, and conductivity. ICP-MS was carried out on an Agilent 4500 Inductively Coupled Plasma Mass Spectrometer. Solid thin film samples were digested in 10 mL 2% (v/v) diluted nitric acid to make solutions prior to analysis. Solutions should normally be aqueous, filtered (removing particles >0.45 μm) and with a total dissolved solids content of less than 1000 ppm. Calibrations were obtained using external calibration analysis (a series of standards of known transition element concentrations were prepared to form a linear relationship for calibration). A quality check was done by using an external standard to dilute and measure from a custom bought multi-element solution.

5 Supporting information

A table of the properties of singly and double doped zinc oxide films, SEM images and charts of grain sizes are given as supplementary material available online (DOI: 10.1515/znb-2019-0196).

Acknowledgements: Peter Edwards thanks the Worshipful Company of Armourers and Brasiers for their award of the 2012 Materials Science Venture Prize and for financial support.

References

[1] Ü. Özgür, Ya. I. Alivov, C. Liu, A. Teke, M. A. Reshchikov, S. Doğan, V. Avrutin, S. J. Cho, H. Morkoç, *J. Appl. Phys.* **2005**, *98*, 041301.
[2] P. Singh, R. Kumar, R. K. Singh, *Ind. Eng. Chem. Res.* **2019**, *58*, 17130–17163.
[3] K. Tang, S. L. Gu, J. D. Ye, S. M. Zhu, R. Zhang, Y. D. Zheng, *Chin. Phys. B.* **2017**, *26*, 047702.
[4] O. Edynoor, A. R. M. Warikh, T. Moriga, K. Murai, M. E. A. Manaf, *Rev. Adv. Mater. Sci.* **2017**, *49*, 150–157.
[5] N. Rashidi, V. L. Kuznetsov, J. R. Dilworth, M. Pepper, P. J. Dobson, P. P. Edwards, *J. Mater. Chem. C.* **2013**, *1*, 6960–6969.
[6] N. Rashidi, A. T. Vai, V. L. Kuznetsov, J. R. Dilworth, P. P. Edwards, *Chem. Commun.* **2015**, *51*, 9280–9283.
[7] A. T. Vai, V. L. Kuznetsov, H. Jain, D. Slocombe, N. Rashidi, M. Pepper, P. P. Edwards, *Z. Anorg. Allg. Chem.* **2014**, *640*, 1054–1062.
[8] A. T. Vai, V. L. Kuznetsov, J. R. Dilworth, P. P. Edwards, *J. Mater. Chem. C.* **2014**, *2*, 9643–9652.
[9] A. T. Vai, N. Rashidi, Y. Fang, V. L. Kuznetsov, P. P. Edwards, *J. Phys.: Condens. Matter.* **2016**, *28*, 224003.
[10] J. Clatot, G. Campet, A. Zeinert, C. Labrugère, M. Nistor, A. Rougier, *Sol. Energy Mater. Sol. Cells.* **2011**, *95*, 2357–2362.
[11] T. Minami, H. Sato, H. Nanto, S. Takata, *Jpn. J. Appl. Phys., Part 2.* **1986**, *25*, L776–L779.
[12] A. K. Das, P. Misra, L. M. Kukreja, *J. Phys. D: Appl. Phys.* **2009**, *42*, 165405.
[13] J. T. Luo, X. Y. Zhu, G. Chen, F. Zeng, F. Pan, *Appl. Surf. Sci.* **2012**, *258*, 2177–2181.
[14] I. Sorar, D. Saygin-Hinczewski, M. Hinczewski, F. Z. Tepehan, *Appl. Surf. Sci.* **2011**, *257*, 7343–7349.
[15] W. Korner, C. Elsässer, *Phys. Rev. B.* **2011**, *83*, 205306.
[16] R. Chowdhury, P. Rees, S. Adhikari, F. Scarpa, S. P. Wilks, *Phys. B* **2010**, *405*, 1980–1985.
[17] R. Dounia, A. Migalska-Zalas, M. Addou, J. C. Bernede, A. Outzourhit, M. Benbrahim, *Opt. Quantum Electron.* **2016**, *48*, 339.
[18] S. Edinger, N. Bansal, M. Bauch, R. A. Wibowo, G. Ujvari, R. Hamid, G. Trimmel, T. Dimopoulos, *J. Mater. Sci.* **2017**, *52*, 8591–8602.
[19] S. Ilican, Y. Caglar, M. Caglar, B. Demirci, *J. Optoelectron. Adv. Mater.* **2008**, *10*, 2592–2598.
[20] V. K. Jayaraman, A. M. Alvarez, M. Bizarro, M. D. O. Amador, *J. Mater. Sci.: Mater. Electron.* **2018**, *29*, 15321–15328.
[21] C. H. Lee, K. S. Lim, J. S. Song, *Sol. Energy Mater. Sol. Cells* **1996**, *43*, 37–45.
[22] A. Maldonado, M. D. L. Olvera, S. T. Guerra, R. Asomoza, *Sol. Energy Mater. Sol. Cells* **2004**, *82*, 75–84.
[23] A. Maldonado, M. D. L. Olvera, R. Asomoza, S. Tirado-Guerra, *J. Mater. Sci.: Mater. Electron.* **2001**, *12*, 623–627.
[24] M. Mikawa, T. Moriga, Y. Sakakibara, Y. Misaki, K. Murai, I. Nakabayashi, K. Tominaga, *Mater. Res. Bull.* **2005**, *40*, 1052–1058.
[25] S. Major, K. L. Chopra, *Sol. Energy Mater.* **1988**, *17*, 319–327.
[26] H. Czternastek, A. Brudnik, M. Jachimowski, *Solid State Commun.* **1988**, *65*, 1025–1029.
[27] Y. Lim, N. Hwang, J. Lee, S. Lee, M. Yi, *J. Nanosci. Nanotechnol.* **2019**, *19*, 1470–1473.
[28] E. Chong, Y. S. Chun, S. Y. Lee, *Appl. Phys. Lett.* **2010**, *97*, 102102.
[29] A. V. Ghule, K. Ghule, C. Chen, W. Chen, S. Tzing, H. Chang, Y. Ling, *J. Mass Spectrom.* **2004**, *39*, 1202–1208.
[30] G. Ambrozic, I. Djerdj, S. D. Skapin, M. Zigon, Z. C. Orel, *CrystEngComm* **2010**, *12*, 1862–1868.
[31] H. Fujiwara, M. Kondo, *Phys. Rev. B* **2005**, *71*, 075109.
[32] J. A. Woollam Co., Inc., *Guide to Using WVASE 32: Spectroscopic Ellipsometry Data Acquisition and Analysis Software*, J. A. Woollam Co., Inc., Lincoln, NE (USA) **2005**, pp. 1–675.
[33] M. A. Lucio-Lopez, A. Maldonado, R. Castanedo-Perez, G. Torres-Delgado, M. D. Olvera, *Sol. Energy Mater. Sol. Cells* **2006**, *90*, 2362–2376.

Brought to you by | UCL - University College London
Authenticated
Download Date | 2/18/20 6:41 PM

[34] T. Yamada, H. Makino, N. Yamamoto, T. Yamamoto, *J. Appl. Phys.* **2010**, *107*, 123534.
[35] Y. Fang, *Singly and Co-Doping of ZnO Thin Films by Spray Pyrolysis*, University of Oxford, Oxford **2018**.
[36] X. H. Zhou, Q. H. Hu, Y. Fu, *J. Appl. Phys.* **2008**, *104*, 063703.
[37] A. C. Galca, G. Socol, V. Craciun, *Thin Solid Films* **2012**, *520*, 4722–4725.
[38] R. Swanepoel, *J. Phys. E: Sci. Instrum.* **1980**, *16*, 1214–1219.
[39] G. Haacke, *J. Appl. Phys.* **1976**, *47*, 4086–4089.

Supplementary Material: The online version of this article offers supplementary material (https://doi.org/10.1515/znb-2019-0196).

Brought to you by | UCL - University College London
Authenticated
Download Date | 2/18/20 6:41 PM